Rotating Superfluid Turbulence

Makoto Tsubota,[1] Tsunehiko Araki,[1] and Carlo F. Barenghi[2]
[1]*Department of Physics, Osaka City University, Sumiyoshi-Ku, Osaka 558-8585, Japan*
[2]*School of Mathematics and Statistics, University of Newcastle, Newcastle upon Tyne NE1 7RU, United Kingdom*
(Received 22 January 2003; published 23 May 2003)

Almost all studies of vortex states in helium II have been concerned with either ordered vortex arrays or disordered vortex tangles. This work numerically studies what happens in the presence of both rotation (which induces order) and thermal counterflow (which induces disorder). We find a new statistically steady state in which the vortex tangle is polarized along the rotational axis. Our results are used to interpret an instability that was discovered experimentally by Swanson *et al.* [Phys. Rev. Lett. **50**, 190 (1983)] and the vortex state beyond the instability that has been unexplained until now.

DOI: 10.1103/PhysRevLett.90.205301 PACS numbers: 67.40.Vs, 03.75.Lm, 47.37.+q

Most configurations of quantized vortices [1] that have been investigated in helium II can be grouped into two types: ordered vortex arrays and disordered vortex tangles. An ordered array is made when helium II is rotated with angular velocity Ω exceeding a certain small critical value. The resulting quantized vortices are aligned along the rotation axis and form an array whose areal number density is given by Feynman's rule $L_{\rm rot} = 2\Omega/\kappa$, where $\kappa = 9.97 \times 10^{-4}$ cm^2/sec is the quantum of circulation. A spatially disordered tangle is obtained [2,3] when helium is made turbulent under thermal counterflow velocity $V_{\rm ns}$ faster than some small critical value, or, more in general [4], using grids [5] or propellers [6]. In this work we concentrate on counterflow because this form of turbulence is simpler (no need to worry about large scale motion and effects induced by normal fluid eddies). In turbulent counterflow the vortex line density (length of vortex line per unit volume) is $L_{\rm flow} = \gamma_H^2 V_{\rm ns}^2$, where γ_H is a temperature-dependent coefficient [3]. This vortex system is almost isotropic, provided that one neglects a small anisotropy induced by the imposed counterflow [7].

An important question naturally arises: What happens if vortices are created by *both* rotation and counterflow along the rotational axis? We are aware of only one experiment which addressed this issue, which was performed by Swanson, Barenghi, and Donnelly [8] years ago. The counterflow channel was mounted on a rotating cryostat, so it was possible to create vortices by independent combination of rotation and counterflow. The absolute value of the vortex line density L was determined from the measurement of the attenuation of a second sound along the channel, which was calibrated against the known density in rotation [9]. Swanson *et al.* found that at slow rotation the critical counterflow velocity above which the flow became turbulent was greatly reduced. Furthermore, two critical velocities V_{c1} and V_{c2} were observed. For $V_{\rm ns} < V_{c1}$ the measured vortex line density $L = L_{\rm rot}$ was independent of the small values of $V_{\rm ns}$ and in agreement with Feynman's rule, which was evidence for an ordered vortex array. The value of V_{c1} was consistent with the critical velocity of a vortex wave instability which had been first observed by Cheng *et al.* [10] and then explained by Glaberson *et al.* [11]. This instability, hereafter referred to as the Donnelly-Glaberson (DG) instability, takes the form of Kelvin waves (helical displacements of the vortex cores), which are destabilized by the component of the counterflow velocity in the direction along the vortices.

Unfortunately, it was not clear to Swanson *et al.* [8] what the nature of the flow was beyond the DG instability ($V_{\rm ns} > V_{c1}$). Their experiment showed that rotation added fewer than the expected $2\Omega/\kappa$ vortex lines to those made by the counterflow. Lacking any direct flow visualization the nature of the flow was a mystery. Theoretically, the linear stability analysis of Glaberson determines only the value V_{c1} of the instability of the vortex array. What happens beyond the instability can be studied only by nonlinear analysis. Thus the pioneering experiment of Swanson *et al.* has lacked a theoretical interpretation.

Motivated by their work, we study numerically quantized vortices under both rotation and counterflow using the vortex filament model. First we prepare an initial vortex array in rotation; then we apply a counterflow $V_{\rm ns}$ along the rotational axis. We find that when $V_{\rm ns} > V_{c1}$ Kelvin waves are excited and grow (DG instability), and the vortex array becomes unstable. Then we show the first numerical evidence for a polarized vortex tangle (polarized superfluid turbulence).

Our work is relevant to other contexts of current interest, such as superfluid ^{3}He and atomic Bose-Einstein condensates [12,13]. In general, our problem is concerned with the competition between order (here induced by rotation) and disorder (here induced by the heat flow).

For superfluid ^{4}He, the vortex filament model is very useful, because the vortex core radius $a_0 \sim 10^{-8}$ cm is microscopic and the circulation $\kappa = 9.97 \times 10^{-4}$ cm^2/sec is fixed. Neglecting the normal fluid, according to Helmholtz's theorem, a superfluid vortex at a point moves with velocity which depends on the shape of

the vortex and on the velocity field $\dot{\boldsymbol{s}}_0$ at that point which is induced by other vortices [14]. Therefore, in order to study a rotating tangle, we need to formulate the laws of vortex dynamics in a rotating frame [15].

The natural way to perform the calculation in a rotating frame would require one to consider a cylindrical container. We do not follow this approach for two reasons. First, our formulation is implemented using the full Biot-Savart law, not the localized-induction approximation often used in the literature. This would require one to place image vortices beyond the solid boundary to impose the condition of no flow across it. This has been done in Cartesian (cubic) geometry, but it is difficult to do in cylindrical geometry, Second, the original experiment by Swanson *et al.* [8] was carried out in a rotating channel with a square cross section.

In a rotating vessel the equation of motion of vortices is modified by two effects. The first effect is the force acting upon the vortex due to the rotation. According to Helmholtz's theorem, the generalized force acting upon the vortex is balanced by the Magnus force as

$$\rho_s \kappa(\boldsymbol{s}' \times \dot{\boldsymbol{s}}_0) = \frac{\delta F'}{\delta \boldsymbol{s}}, \tag{1}$$

where $F' = F - \boldsymbol{\Omega} \cdot \boldsymbol{M}$ is the free energy of a system in a frame rotating around a fixed axis with angular velocity $\boldsymbol{\Omega}$ and angular momentum $\boldsymbol{M}$. Taking the vector product with $\boldsymbol{s}'$, we obtain the velocity $\dot{\boldsymbol{s}}_0$. The first term F due to the kinetic energy of vortices gives that Biot-Savart law, and the second term $\boldsymbol{\Omega} \cdot \boldsymbol{M}$ leads to the velocity $\dot{\boldsymbol{s}}_{\rm rot}$ of the vortex caused by the rotation. The second effect is the superflow induced by the rotating vessel. For a perfect fluid we know the analytical solution of the velocity $\boldsymbol{v}_{\rm cub}$ inside a cube of size D rotating with angular velocity $\boldsymbol{\Omega} = \Omega \hat{\boldsymbol{z}}$ [16]. By taking into account both effects, we eventually obtain the velocity $\dot{\boldsymbol{s}}_0$ in a rotating frame which is

$$\dot{\boldsymbol{s}}_0 = \frac{\kappa}{4\pi} \boldsymbol{s}' \times \boldsymbol{s}'' \ln\left(\frac{2(l_+ l_-)^{1/2}}{e^{1/4} a_0}\right) + \frac{\kappa}{4\pi} \int' \frac{(\boldsymbol{s}_1 - \boldsymbol{r}) \times d\boldsymbol{s}_1}{|\boldsymbol{s}_1 - \boldsymbol{r}|^3} + \dot{\boldsymbol{s}}_{\rm rot} + \boldsymbol{v}_{\rm cub}, \tag{2}$$

where the first term on the right-hand side is the usual desingularization of the Biot-Savart integral which is well known in the literature. Here the vortex filament is represented by the parametric form $\boldsymbol{s} = \boldsymbol{s}(\xi, t)$. The symbols l_+ and l_- are the lengths of the two adjacent line elements after discretization, and the prime denotes differentiation with respect to the arc length ξ. The second term represents the nonlocal field by carrying out the integral along the rest of the filament on which $\boldsymbol{s}_1$ refers to a point.

At a finite temperature, a quantized vortex is also affected by the mutual friction, as the vortex core is dragged by the normal flow. Taking this effect into account the velocity of a vortex line at the point $\boldsymbol{s}$ is given by

$$\dot{\boldsymbol{s}} = \dot{\boldsymbol{s}}_0 + \alpha \boldsymbol{s}' \times (\boldsymbol{v}_{\rm ns} - \dot{\boldsymbol{s}}_0) - \alpha' \boldsymbol{s}' \times [\boldsymbol{s}' \times (\boldsymbol{v}_{\rm ns} - \dot{\boldsymbol{s}}_0)], \tag{3}$$

where α and α' are the temperature-dependent friction coefficients.

Two quantities are useful for characterizing the rotating tangle. The first is the vortex line density $L = (1/\Lambda) \int d\xi$, where the integral is taken along all vortices in the sample volume Λ. The second is the polarization of the tangle, which we define by $\langle s_z' \rangle = (1/\Lambda) \int d\xi \boldsymbol{s}'(\xi) \cdot \hat{\boldsymbol{z}}$, where $\hat{\boldsymbol{z}}$ is the unit vector along the z direction. Note that $\langle s_z' \rangle$ is unity for a vortex array and zero for a randomly oriented tangle.

We now describe briefly how to perform the numerical calculation [17]. A vortex filament is represented by a single string of points at a distance $\Delta\xi$ apart. When two vortices approach within $\Delta\xi$, they are assumed to reconnect. The computational sample is taken to be a cube of size $D = 1.0$ cm. We adopt periodic boundary conditions along the rotating axis and rigid boundary conditions at the side walls. All calculations are made under the full Biot-Savart law, placing image vortices beyond the solid boundaries. Our space resolution is $\Delta\xi = 1.83 \times 10^{-2}$ cm and the time resolution is $\Delta t = 4.0 \times 10^{-3}$ sec. The counterflow $\boldsymbol{V}_{\rm ns}$ is applied along the z axis. The normal fluid is assumed to be at rest in the rotating frame, and, to make comparison with the experiment [8], we use $\alpha = 0.1$ and $\alpha' = 0$ for the temperature $T = 1.6$ K.

Swanson *et al.* [8] found that the first critical velocity V_{c1} is proportional to $\Omega^{1/2}$, in agreement with the DG instability of Kelvin waves. Glaberson *et al.* [11] modeled a vortex array rotating at angular velocity Ω as a continuum and found that, in the absence of the friction, the angular velocity of the Kelvin wave of wave number k is given by the dispersion relation $\omega = 2\Omega + \nu k^2$, where $\nu = (\kappa/4\pi) \ln(b/a_0)$ and $b \approx L^{-1/2}$ is the average distance between vortices. This dispersion law has a critical velocity $V_{\rm DG} = (\omega/k)_{\rm min} = 2(2\Omega\nu)^{1/2}$ at the critical wave number $k_{\rm DG} = \sqrt{2\Omega/\nu}$. Therefore, if the axial flow $V_{\rm ns}$ exceeds $V_{\rm DG}$ for some value of k, Kelvin waves with that wave number k become unstable and grow exponentially in time. Physically, the phase velocity of the mode k is equal to the axial flow, so energy is fed into the Kelvin wave by the flow.

Figure 1 illustrates the DG instability. The computation was performed with angular velocity $\Omega = 9.97 \times 10^{-3}$ rad/sec, for which $V_{\rm DG} = 0.010$ cm/sec. The vortex lines remain stable when $V_{\rm ns} = 0.008$ cm/sec $< V_{\rm DG}$ [Fig. 1(a)], while at $V_{\rm ns} = 0.015$ cm/sec $> V_{\rm DG}$ Kelvin waves become unstable and grow [Fig. 1(b)], as predicted. Figure 1(c) shows that Kelvin waves of a larger wave number become unstable at higher counterflow velocity.

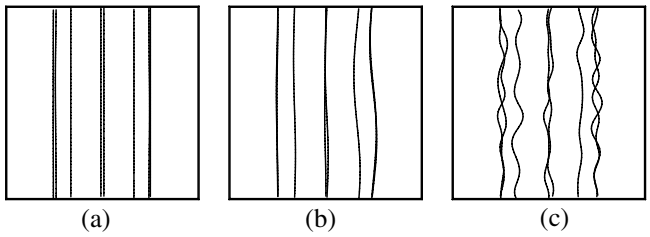

FIG. 1. Numerical simulations of the Donnelly-Glaberson instability at $\Omega = 9.97 \times 10^{-3}$ rad/sec, $T = 1.6$ K. Each snapshot of the vortex configuration is for the counterflow velocity $V_{ns} = 0.008$ cm/sec (a), 0.015 cm/sec (b), and 0.05 cm/sec (c).

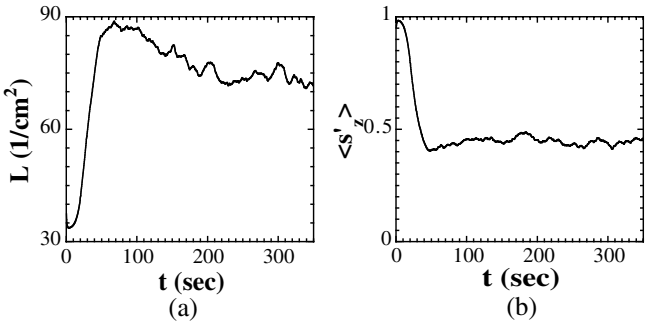

FIG. 3. Time evolution of L (a) and $\langle s_z' \rangle$ (b) at $T = 1.6$ K and $V_{ns} = 0.08$ cm/sec for $\Omega = 4.98 \times 10^{-2}$ rad/sec.

This is the first numerical confirmation of the DG instability in a rotating vortex system.

The key question follows: What happens to the vortices beyond the DG instability? Because of the computational cost of the Biot-Savart law, it is not practically possible to compute vortex tangles with densities which are as high [$L = \mathcal{O}(10^4)$ cm^{-2}] as those achieved in the experiment. Nevertheless, the following numerical simulations can shed light into the physical processes involved. The time sequence contained in Fig. 2 illustrates the evolution of a vortex array at $\Omega = 4.98 \times 10^{-2}$ rad/sec under the counterflow $V_{ns} = 0.08$ cm/sec. Figure 2(a) shows the initial $N = 33$ parallel vortex lines; they have been seeded with small random perturbations to make the simulation more realistic. As the evolution proceeds, perturbations with high wave numbers are damped by friction, whereas perturbations which are linearly DG unstable grow exponentially; hence Kelvin waves become visible [Fig. 2(b)]. When the amplitude of the Kelvin waves becomes of the order of the average vortex separation, reconnections take place [Fig. 2(c)]. The resulting vortex loops disturb the initial vortex array, leading to an apparently random vortex tangle [Fig. 2(d)]. After the initial exponential growth (which is predicted by the theory of the DG instability), nonlinear effects (vortex interactions and vortex reconnections) become important and nonlinear saturation takes place. The two effects are apparent in Fig. 3(a), which shows the initial exponential growth of L (linear instability) and the successive equilibration to a statistical steady state (nonlinear saturation).

Looking carefully at the saturated tangle in Fig. 2(d) we notice that there are more loops oriented vertically than horizontally. Figure 3(b) shows how the polarization $\langle s_z' \rangle$ changes with time in the calculation presented in Fig. 2. During the exponential growth (linear phase) $\langle s_z' \rangle$ decreases from unity (ordered vortex array), but it never becomes zero (random tangle), settling instead to the finite value $\langle s_z' \rangle \approx 0.5$ as soon as nonlinear saturation takes place at about $t \approx 100$ sec.

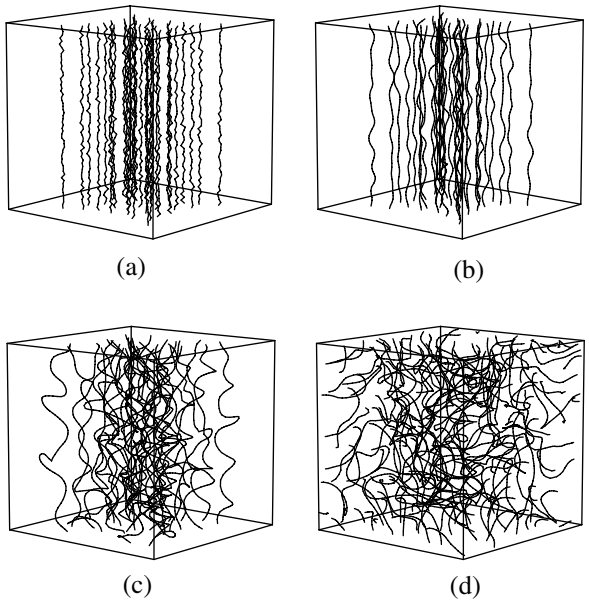

FIG. 2. Numerical simulation of rotating turbulence at $T = 1.6$ K, $\Omega = 4.98 \times 10^{-2}$ rad/sec, and $V_{ns} = 0.08$ cm/sec. Computed vortex tangle at the following times: (a) $t = 0$ sec; (b) $t = 12$ sec; (c) $t = 28$ sec; (d) $t = 160$ sec.

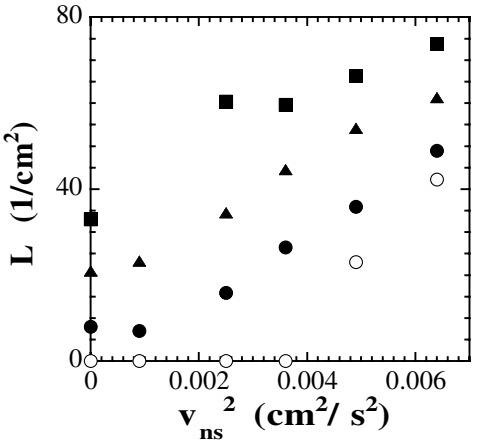

FIG. 4. Vortex line density L vs V_{ns}^2 at $T = 1.6$ K for $\Omega = 0$ (white circles), $\Omega = 9.97 \times 10^{-3}$ rad/sec (black circles), $\Omega = 2.99 \times 10^{-2}$ rad/sec (triangles), and $\Omega = 4.98 \times 10^{-2}$ rad/sec (squares).

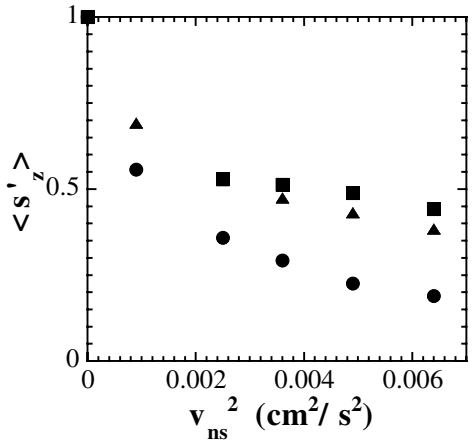

FIG. 5. Tangle's polarization $\langle s_z' \rangle$ vs $V_{\rm ns}^2$ at $T = 1.6$ K for $\Omega = 9.97 \times 10^{-3}$ rad/sec (circles), $\Omega = 2.99 \times 10^{-2}$ rad/sec (triangles), and $\Omega = 4.98 \times 10^{-2}$ rad/sec (squares).

Figure 4 shows the calculated dependence of the vortex line density L on the counterflow velocity $V_{\rm ns}$ at different rotation rates Ω. The dependence of L on $V_{\rm ns}$ is similar to what appears in Fig. 1 of the paper by Swanson *et al.* [8]. The only difference is that the scale of the axes in the paper by Swanson *et al.* is bigger—in this particular figure they report vortex line densities as high as $L \approx 2500$ cm^{-2}, whereas our calculations are limited to $L \approx 80$ cm^{-2}. Despite the lack of overlap between the experimental and numerical ranges, there is clear qualitative similarity between the figures. It is apparent that the critical velocity beyond which L increases with $V_{\rm ns}$ is much reduced by the presence of rotation, which is consistent with the experiment. Figure 5 shows the calculated polarization $\langle s_z' \rangle$ as a function of counterflow velocity $V_{\rm ns}$ at different rotation rates Ω. It is apparent that the polarization decreases with the counterflow velocity and increases with the rotation.

In conclusion, we have numerically studied vortex tangles under the effect of rotation for the first time. At velocities higher than the onset of the DG instability we have determined the existence of a new state of superfluid turbulence (polarized turbulence) that is characterized by two statistically steady state properties, the vortex line density and the degree of polarization. Although the computed range of vortex line densities does not overlap with the much higher values obtained in the experiments, we find the same qualitative dependence of vortex line density versus counterflow velocity at different rotations.

Further work will investigate other aspects of the problem, particularly the nature of V_{c2} and what happens at very high counterflow velocities. We also hope that this work will stimulate more experiments. For example, it should be possible to observe the polarization of turbulence by using simultaneous measurements of second sound attenuation along and across the rotation axis.

The authors thank W. F. Vinen for useful discussions. C. F. B. is grateful to the Royal Society for financially supporting this project. M. T. is grateful to Japan Society for the Promotion of Science for financially supporting this Japan–U.K. Scientific Cooperative Program (Joint Research Project).

[1] R. J. Donnelly, *Quantized Vortices in Helium II* (Cambridge University Press, Cambridge, 1991).
[2] W. F. Vinen, Proc. R. Soc. London A **242**, 493 (1957); **243**, 400 (1958).
[3] J. T. Tough, in *Progress in Low Temperature Physics*, edited by D. F. Brewer (North-Holland, Amsterdam, 1981), Vol. 8.
[4] W. F. Vinen and J. J. Niemela, J. Low Temp. Phys. **129**, 213 (2002).
[5] S. R. Stalp, L. Skrbek, and R. J. Donnelly, Phys. Rev. Lett. **82**, 4831 (1999).
[6] J. Maurer and P. Tabeling, Europhys. Lett. **43**, 29 (1998).
[7] R. T. Wang, C. E. Swanson, and R. J. Donnelly, Phys. Rev. B **36**, 5240 (1987).
[8] C. E. Swanson, C. F. Barenghi, and R. J. Donnelly, Phys. Rev. Lett. **50**, 190 (1983).
[9] C. F. Barenghi, K. Park, and R. J. Donnelly, Phys. Lett. **84A**, 453 (1981).
[10] D. K. Cheng, M. W. Cromar, and R. J. Donnelly, Phys. Rev. Lett. **31**, 433 (1973).
[11] W. I. Glaberson, W. W. Johnson, and R. M. Ostermeier, Phys. Rev. Lett. **33**, 1197 (1974); R. M. Ostermeier and W. I. Glaberson, J. Low Temp. Phys. **21**, 191 (1975).
[12] C. F. Barenghi, R. J. Donnelly, and W. F. Vinen, *Quantized Vortex Dynamics and Superfluid Turbulence* (Springer-Verlag, Berlin, Heidelberg, New York, 2001).
[13] J. R. Abo-Shaeer, C. Raman, and W. Ketterle, Phys. Rev. Lett. **88**, 070409 (2002); V. Bretin, P. Rosenbusch, F. Chevy, G. V. Shlyapnikov, and J. Dalibard, cond-mat/0211101.
[14] K. W. Schwarz, Phys. Rev. Lett. **49**, 283 (1982); Phys. Rev. B **31**, 5782 (1985); **38**, 2398 (1988).
[15] M. Tsubota and H. Yoneda, J. Low Temp. Phys. **101**, 815 (1995).
[16] L. M. Milne-Thomson, *Theoretical Hydrodynamics* (Macmillan, London, 1968), 5th ed., p. 271.
[17] M. Tsubota, T. Araki, and S. K. Nemirovskii, Phys. Rev. B **62**, 11751 (2000).